Direct Observation of Local Distortion of a Crystal Lattice with Picometer Accuracy Using Atomic Resolution Neutron Holography

L. Cser,[1,*] G. Krexner,[2] M. Markó,[1,3] I. Sharkov,[4] and Gy. Török[1]

[1]*Neutron Spectroscopy Department, Research Institute for Solid State Physics and Optics, P.O.B. 49, H-1525, Hungary*
[2]*Institute of Experimental Physics, University of Vienna, Boltzmanngasse 5, A-1090 Vienna, Austria*
[3]*Institute of Nuclear Technics, Budapest University of Technology and Economics, Műegyetem rakpart 1, H-1113 Budapest, Hungary*
[4]*St. Petersburg State University, Institute of Physics, Chair of Optics and Spectroscopy, Ulyanovskaja str.1, 198904 St.Petersburg, Russia*

(Received 12 September 2006; published 19 December 2006)

We demonstrate that neutron holography permits us to extend the determination of atomic positions beyond nearest neighbors at least up to the fourth neighboring shell around cadmium probe atoms alloyed into a lead crystal. The accuracy achieved is sufficient to allow quantitative determination of displacements of atoms due to elastic distortions induced by impurity atoms. The atomic positions derived from the holographic data are in good agreement with those expected theoretically due to Friedel oscillations in this system. In addition, the atomic positions are in qualitative agreement with results obtained in an independent experiment studying the diffuse distortion scattering around Bragg peaks.

DOI: 10.1103/PhysRevLett.97.255501 PACS numbers: 61.72.−y, 61.12.−q, 61.18.−j, 61.66.Dk

Impurity atoms embedded in a regular host lattice generally give rise to local lattice distortions. If the induced atomic displacements occur on surfaces, they can, at least in principle, be viewed directly. Yet, in the bulk usually one has to draw on indirect evidence, and there is no practical way to unambiguous determination of lattice distortions due to single atoms. One of the commonly accepted approaches to their study is diffuse x-ray or neutron scattering around Bragg peaks [1]. However, this method is based on the continuum approximation and, therefore, provides information about averaged distortions on the nanoscale [2] while it breaks down in the immediate neighborhood of the defect where the atomistic structure of the lattice has to be taken into account. The interpretation is intimately related to the semimacroscopic notion of the displacement field [3] and gives quantitative results only at a certain distance from the impurity. The determination of the displacements of individual atoms belonging to the closest atomic shells surrounding the impurity requires an experimental approach with higher resolution. Theoretically, a reconstruction of the atomic positions would be feasible by scanning the elastic diffuse scattering intensity in large regions of reciprocal space and calculating its Fourier transform. *In praxi*, however, the accessible momentum range is strongly restricted, and, consequently, experimental data can be compared only with calculations based on preconceived models.

Presenting a novel approach, atomic resolution neutron holography provides detailed information about the positions of individual atoms surrounding probe nuclei in the bulk. In a previous paper [4], the successful reconstruction of the 3D holographic image of the first neighboring shell of Cd impurity atoms occupying regular lattice sites in a single crystal of lead was described. At that time, the main goal of the experiment was to demonstrate the feasibility of the concept of atomic resolution neutron holography. In the present Letter, we report on a precise determination of the positions of about 50 individual lead atoms making up the first four neighboring shells surrounding the Cd atom. The composition of the sample was $Pb_{99.74}Cd_{0.26}$ (i.e., nearly 400 Pb atoms for one Cd atom) so that the Cd atoms can be considered as noninteracting impurity atoms on an fcc lattice of lead atoms [4].

Applying the Helmholtz-Kirchhoff transformation [5] to the experimental data, the positions of the lead atoms in the first, second, third and fourth neighboring shell were recognized and identified. The results are shown in Fig. 1. In contrast to X-ray holography which provides images of the electronic shells, the nuclei become visible in a neutron experiment. The successful holographic imaging of atomic positions beyond the nearest neighbors was achieved in this experiment for the first time. For simplicity, only the maximum value of the restored hologram intensity as a function of the distance from the Cd nucleus was considered (see Fig. 2). In Fig. 1, the first, third, and fourth neighbors are clearly visible on the oscillating background. In the case of the second neighbors, however, the intensity of the experimental spots associated with the position of nuclei is comparable with the background oscillations. According to model calculations which were carried out on the supposition that all Pb atoms in the PbCd sample occupy the same positions as in the pure Pb crystal, the intensity of the second neighbors is even higher than that of the first one. This fact is a serious argument in favor of the hypothesis that the local arrangement of the crystal is deformed due to the presence of alloyed Cd. In order to explain the deviation of the observed intensities from the calculated ones, let us consider the following arguments: The holographic term of the scattering intensity distribution is [5]

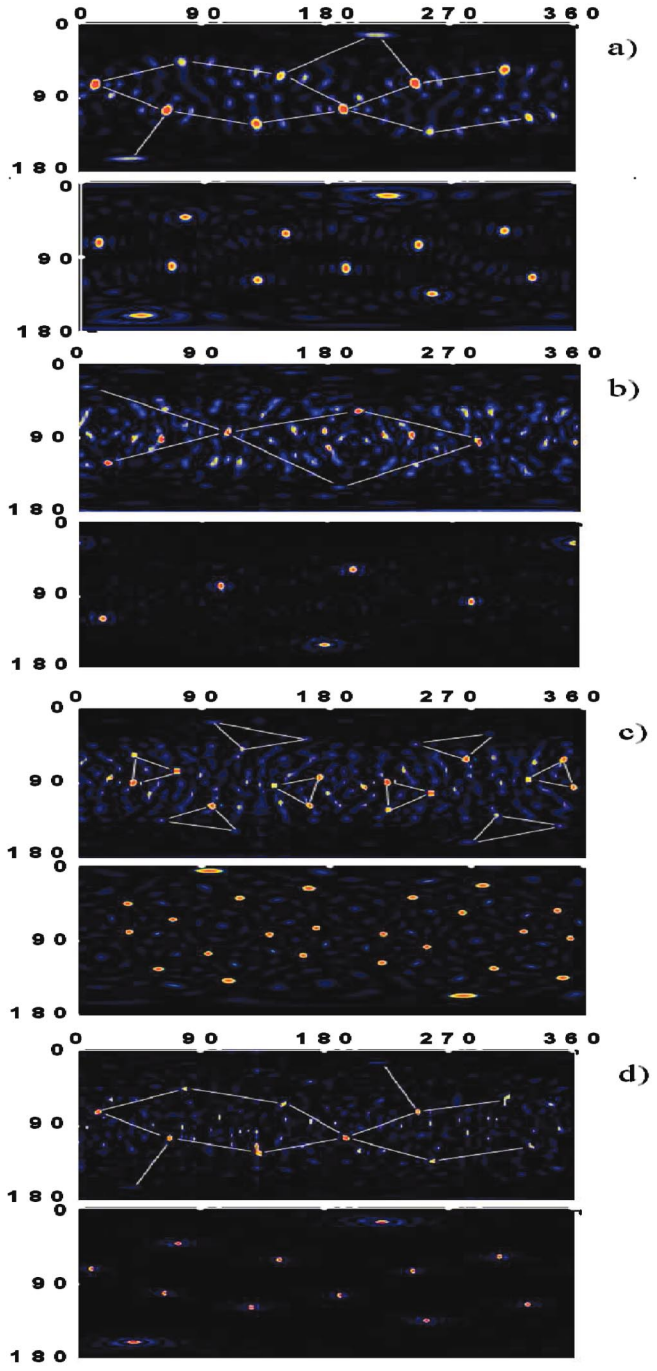

FIG. 1 (color). (a)–(d): Reconstructions of the four closest shells of neighboring atoms around a Cd probe nucleus. Each figure shows (top) an intensity map obtained from the hologram recorded in the experiment and connecting lines pointing out high-intensity spots, (bottom) a numerical simulation of the expected map. The angle coordinates ϕ (0–360°) and χ (0–180°) define the positions on spherical surfaces around the probe nucleus. The Pb atoms form an fcc lattice; thus, the four shells contain 12, 6, 24, and 12 atoms, respectively.

$$\chi(\mathbf{k}) = 2\sum_i \frac{b_i}{r_i}\cos(kr_i - \mathbf{kr}_i). \quad (1)$$

Here b_i are the scattering amplitudes, $\mathbf{k}$ denotes the momentum transfer, and $\mathbf{r}_i$ stands for the positions of the scattering nuclei (the index i enumerates all atoms contributing to the hologram). For nuclei n and m occupying symmetrical positions $\mathbf{r}_n = -\mathbf{r}_m$. This relation allows rewriting Eq. (1) separating the symmetrical pairs in the form

$$\chi(\mathbf{k}) = 2\sum_n \frac{b_n}{r_n}[\cos(kr_n - \mathbf{kr}_n) + \cos(kr_n + \mathbf{kr}_n)] \quad (2)$$

where the summation now is made over one half of the atoms. Using a simple trigonometric transformation

$$\chi(\mathbf{k}) = 4\sum_n \frac{b_n}{r_n}\cos(kr_n)\cos(\mathbf{kr}_n). \quad (3)$$

In order to obtain the reconstructed hologram, we apply the Helmholtz-Kirchhoff transformation

$$U(\mathbf{R}) = \int_{\sigma_k} \chi(\mathbf{k}) e^{i\mathbf{kr}_n} d\sigma_k = 4\sum_n \frac{b_n}{r_n}\cos(kr_n)\int_{\sigma_k}\cos(\mathbf{kr}_n)e^{i\mathbf{kr}_n}d\sigma_k. \quad (4)$$

The observed intensity of the reconstructed hologram is obtained from the squared absolute value of $U(\mathbf{R})$.Then Eq. (4) gets separated into the product of two terms. The first one reflects the modulation of the maximum value of the intensity proportionally to

$$I(\mathbf{R}) = |U(\mathbf{R})|^2 \sim \left[\frac{\cos(kr_n)}{r_n}\right]^2. \quad (5)$$

The integral forming the second term describes the shape of the given peak. The intensity variation according to Eq. (5) is illustrated in Fig. 3. Relation (5) allows us to obtain the positions of the holographic spots, i.e., the positions of the Pb nuclei, from the variation of the peak intensity maximum. Unfortunately, the distance dependence of this value shown in Fig. 3 is not normalized.

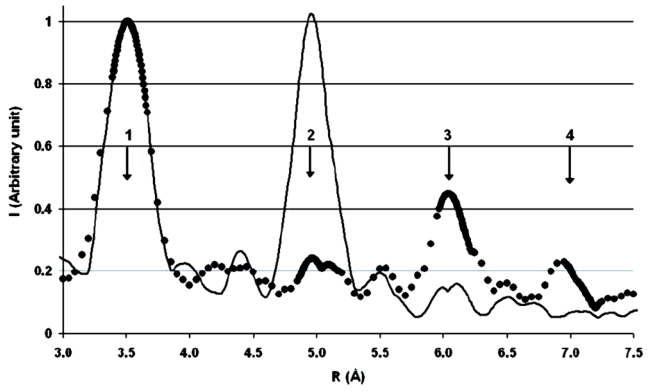

FIG. 2 (color online). The maximum intensity distribution of the restored holographic image as a function of the distance R from the Cd nucleus. Experimental values (●), model calculation for a nondistorted crystal involving 100 surrounding shells (continuous line). The intensity is normalized to the first peak. Vertical arrows mark the positions of atoms in a nondistorted lead crystal. Oscillations between the peaks are inherent to the holographic restoring procedure [10].

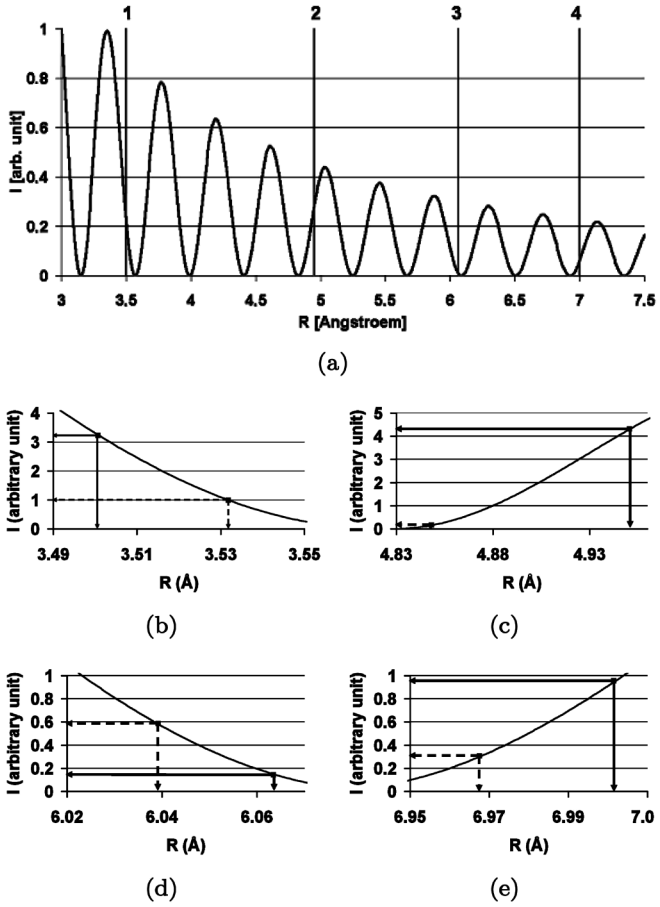

FIG. 3. (a) The variation of the holographic intensity as a function of the distance R from the probe atom calculated using Eq. (5). The vertical solid lines show the expected positions of the lead atoms for the perfect crystal. Figs. (b), (c), (d), and (e) show a close-up view of the vicinity of the 1st, 2nd, 3rd, and 4th neighbors, respectively. The vertical dashed lines show the real positions of the lead atoms obtained from the experimental data.

This means that, from the experimental data, we are able to determine only the ratio of the maximum values. In order to overcome this obstacle, we carried out a numerical fit of three-dimensional Gaussians $G(\chi, \phi, R)$ to the independent peaks belonging to the first neighbors—both for the experimental results and the model calculation—and accepted the positions of the maxima of the Gaussians as the positions of the holographic spots. Since the points to be fitted are statistically not independent, the quality of the fit was characterized by the coefficient of determination amounting in our case to 0.99962. (This quantity—usually marked as R^2—shows how close the points are to the Gaussian line.) Using this procedure, all independent positions of first neighbors were obtained. Their average value is equal to 3.5318 ± 0.0024 Å. The error was calculated as the standard deviation from this average value. The oscillations appearing in the model calculation due to the rather small number of shells taken into account do not allow to apply a similar approach to more distant neighbors, amongst others because the intensity of these peaks is much smaller than that of the first shell. Yet, starting from the result for the first neighbors, we can determine the relation between their position and intensity, and from the intensity ratio between the first and the other three neighbors, one can calculate their positions using Eq. (5). In our case $\lambda = 0.84$ Å, thus $|k| = 2\pi/\lambda = 7.48$ Å^{-1}. The results are given in Table I.

From the data given in Table I, it is clear that the displacement varies non-monotonically with increasing number of shells. For the explanation of this observation, we propose the following reasoning:

There are two effects the balance of which determines the perturbation of interatomic distances actually found. One is the ratio of the atomic radii, and the second is an electrostatic force deriving from the valence difference of the host and the impurity atoms. The atomic radius calculated from the bond length of Pb is equal to 175 pm, while that of Cd is 149 pm [6]. The ratio of these two values would favor a contraction of the next neighbor distance; however, the experimental data for the first neighbors actually show an increase. From that we conclude that the electrostatic force is dominating over the size effect. Indeed, the outer shell of a Cd atom consists of $5s^2$ electrons while the lead atom has the electron configuration $6s^2 6p^2$. This results in a charge depletion at the position of the Cd atom which is equal to -2. In other words, by using a simple qualitative explanation, we can tell that Cd atoms embedded in the Pb lattice carry a negative extra charge causing a repulsive force acting on the p electrons of the first neighboring lead atoms. As a result, the whole Pb atom suffers a repulsion leading to an increase of the Pb-Cd distance.

This fact immediately suggests to apply Friedel's theory [7,8]. In this approach, the conduction electrons of lead scatter at the extra charge of the impurity (in the present case on the Cd atom) and form an oscillating charge distribution around it [9]. In Fig. 4, the oscillating term

TABLE I. Intensity of the holographic signal of the first four neighbor shells around a Cd probe atom and the corresponding displacements from their positions in a perfect lead crystal. All distances are given in Å.

neighbor shell	relative intensity	observed position	undistorted position	shift
1	1	3.5318	3.5007	0.0311 ± 0.002
2	0.155	4.8481	4.9508	-0.1027 ± 0.011
3	0.583	6.0392	6.0635	-0.0243 ± 0.011
4	0.301	6.9676	7.0015	-0.0339 ± 0.013

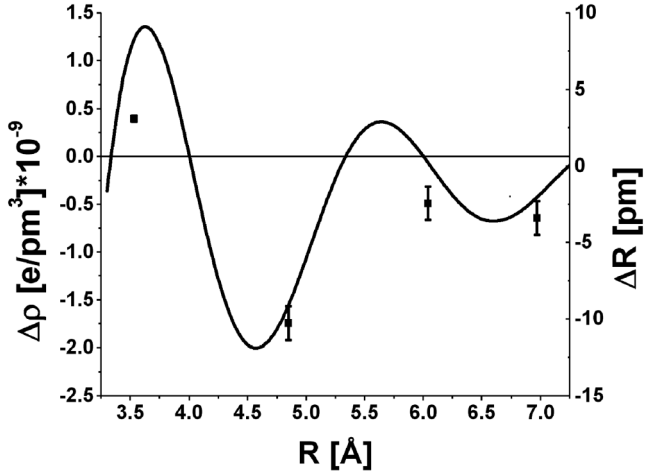

FIG. 4. Continuous line: calculated electron density modulation around a Cd atom (refer to left scale). Black squares: experimentally observed local distortion as a function of the distance from the Cd nucleus (refer to right scale). The error bars are estimated from the average value of the oscillations modulating the background line.

of the p electrons of the lead atoms is displayed as calculated using Friedel's description. At the position of the first neighbor shell formed by lead atoms surrounding the Cd impurity, the electron density modulation $\Delta\rho(R)$ has a positive sign which means also that a repulsive force appears between Cd and Pb atoms in accordance with the expectation based on the foregoing qualitative consideration. Concerning the more distant neighbors, the variation of the Cd-Pb distance is also following the charge density curve (see the black squares in Fig. 4). As a consequence, the correlation between the charge density oscillation and the Cd-Pb distance variation becomes obvious. Evidently, the forces caused by the electron density variation around the Cd atom are dominating over the simple internal stress effect due to the size difference. Nevertheless, Fig. 4 shows that the average local deformation of the first four shells around the Cd atom is dominantly contractive.

From the above, one has to expect a Huang-type neutron diffuse scattering pattern close to Bragg peaks. A test measurement of the diffuse scattering carried out at the ATHOS three axis spectrometer installed at the Budapest Research Reactor clearly demonstrates the presence of such a contribution. Because of the available experimental conditions, the diffuse scattering data obtained close to the (200) reflection were not obtained in purely radial direction, so that this measurement cannot provide a quantitative evaluation of the contraction. Obviously, a more detailed study has to be devoted to the diffuse scattering. However, much stronger diffuse scattering is found on the high-Q side of the Bragg peak, which is a clear indication of a zone of compression around the core of the distortion field, which is qualitatively in agreement with the above results based on the holographic data and interpreted as a Friedel oscillation.

In conclusion, we underline that using neutron holography, we have entered the range of interatomic distance measurements which is not accessible to conventional diffuse scattering, neither with x rays nor neutrons. This method provides information about the local lattice distortion on an atomic scale. The very fact that there is a direct connection between the intensity of the holographic peaks and their position provides a new approach to the measurement of atomic distances. Moreover, from the relationship (5), it can be immediately seen that by proper choice of the wavelength, the intensity for a particular neighboring shell can be adjusted in such a way as to coincide with the zone of steepest slope in the dependence on the product (kr). Thus, the intensity variation of the holographic spot may serve as a very sensitive probe for detecting the change of the interatomic distances either under external influences such as pressure, temperature, magnetic field, etc., or, e.g., due to a phase transition.

The authors are indebted to the Stiftung Aktion Österreich-Ungarn (AÖU), to the Austrian Science Fund FWF (No. P16596-N02), and to the NAP No. VENEUS05 Project for valuable support.

*Electronic address: cser@sunserv.kfki.hu

[1] P. H. Dederichs, J. Phys. F **3**, 471 (1973).
[2] G. Krexner, M. Prem, F. Beuneu, and P. Vajda, Phys. Rev. Lett. **91**, 135502 (2003).
[3] M. A.Krivoglaz, *X-ray and Neutron Diffraction in Nonideal Crystals* (Springer-Verlag, Berlin, Heidelberg, New York, 1996).
[4] L. Cser, Gy. Török, G. Krexner, I. Sharkov, and B. Faragó, Phys. Rev. Lett. **89**, 175504 (2002).
[5] J. J. Barton, Phys. Rev. Lett. **61**, 1356 (1988).
[6] WebElements™ Periodical table (professional edition), www.webelements.com (2004).
[7] J. Friedel, Philos. Mag. **43**, 153 (1952).
[8] C. Kittel, *Quantum Theory of Solids* (John Wiley & Sons, New York, 1963).
[9] L. Cser, I. Gladkih, and Cs. Hargitai, Phys. Status Solidi B **124**, 271 (1984).
[10] M. Markó, L. Cser, G. Krexner, I. Sharkov, Physica B (Amsterdam) (to be published).